

Solubilization of *n*-alkanes into polyazomethines having flexible (*n*-alkyloxy)methyl side chains

Heesub Kim, Jin Chul Jung and Wang-Cheol Zin*

Department of Materials Science and Engineering, Pohang University of Science and Technology, San 31, Hyoja-dong, Pohang, 790-784 Korea
 (Received 18 April 1995)

Solubilization behavior of *n*-alkanes (C_k , $k = 15, 20, 32, 40$ and 50) into polyazomethines (C_m -PAM) having flexible (*n*-alkyloxy)methyl side chains ($-\text{CH}_2\text{OC}_m\text{H}_{2m+1}$, $m = 4, 6, 8, 12$) was studied by measuring layer spacings of the layered structures with wide-angle X-ray scattering (WAXS) and effects of side chain lengths of the polymers and chain lengths of *n*-alkanes were discussed. Liquid *n*-alkanes were miscible with the side chains of the polymers only when the side chains were molten to form mesophase. In mesophase the layered structure was not disrupted by adding C_k and on adding excess *n*-alkanes the presence of solubility limits was confirmed. With increasing side chain length of C_m -PAM and chain length of C_k the solubility limit of *n*-alkane increased and decreased, respectively. Copyright © 1996 Elsevier Science Ltd.

(Keywords: polyazomethines; *n*-alkane; solubilization)

INTRODUCTION

As already demonstrated in a number of recent reports^{1–12}, solubility of rigid-rod polymers are remarkably enhanced by appending flexible side chains to the backbone, since the side chains act as a bound solvent² toward the rigid main chain. The appendage of flexible side chains leads the polymers to forming a unique liquid crystalline phase at temperature where thermal degradation does not prevail. The layered mesophase is formed in the polymers with sufficiently long side chains and readily identified by a strong Bragg reflection appearing in the small-angle region. The phase behaviour of these rigid-rod polymers is mainly governed by the strong segregation of main chain domain from side chain domain, being analogous to the microphase separation of block copolymers.

In our recent papers^{13,14}, we have reported the preparation, crystal structure and phase behaviour of aromatic polyazomethines with (*n*-alkyloxy)methyl side chains with various lengths. The polyazomethines had been prepared by condensation of 2,5-bis[(*n*-alkyloxy)methyl]terephthalaldehydes with *p*-phenylenediamine¹³.

For molecular packing of C_m -PAM at room temperature a layered structure has been suggested as a model crystal structure in our previous report¹⁴. In this structure the rigid main chains form layers and the flexible side chains emanating from the layers fill the space between the layers. Structural changes taking place by phase transitions identified in d.s.c. studies were investigated for the unoriented samples by temperature-controlled WAXS in greater detail. In the proper temperature range all the polymers were confirmed to

form mesophases, in which the highly ordered layered structure still remained undisrupted. When the side chains interdigitated with each other between rigid backbone layers they were molten to form mesophase. *n*-Alkanes having chemically similar structure with the side chains became miscible with them and penetrated into their domain, thereby increasing the layer spacing between backbone layers.

In the present work we present solubilization behaviour of *n*-alkanes (C_k , $k = 15, 20, 32, 40, 50$) into polyazomethines having (*n*-alkyloxy)methyl side chains (C_m -PAM, $m = 4, 6, 8, 12$). It was studied by measuring changes in layer spacing by means of WAXS at various temperatures.

EXPERIMENTAL

Samples of C_m -PAM and C_k were in powder form. Blends were prepared by adding specified weights of C_k to C_m -PAM under vigorous stirring at temperatures above crystal–mesophase transitions of C_m -PAM in vacuum. WAXS measurements were made in transmission mode in the $2^\circ < 2\theta < 35^\circ$ range using $\text{CuK}\alpha$ radiation and a graphite monochromator installed in front of the counter. All diffractograms are used as observed. For *in situ* measurements at various temperatures a heating stage with electric heater was used. For prevention of the molten samples from flowing down the sample powders were windowed with Kapton film and the scattering intensity from the Kapton window was subtracted.

RESULTS AND DISCUSSION

The X-ray diffractograms of pure C_{12} -PAM and

* To whom correspondence should be addressed

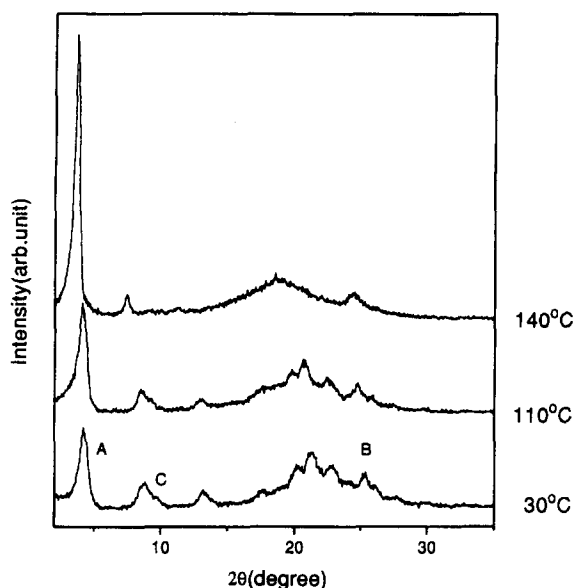


Figure 1 X-ray diffractogram of C_{12} -PAM taken at different temperatures

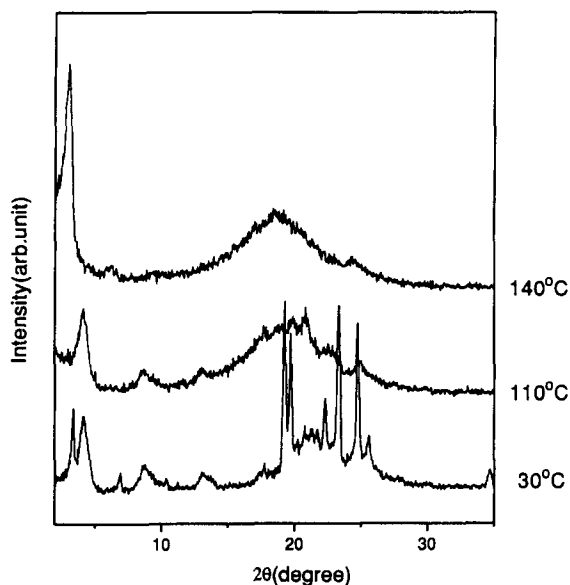


Figure 2 X-ray diffractogram of C_{20}/C_{12} -PAM blend taken at different temperatures

C_{20}/C_{12} -PAM blend (1/1 w/w) taken at different temperatures are reproduced in Figures 1 and 2, respectively. Detailed interpretation of the peaks of Figure 1 designated as A, B and C leading to a layered structure has already been described previously¹⁴. The reflections A, B and C arise from layer spacing, lateral backbone spacing and slipped repeat unit, respectively.

Compared with Figure 1, the X-ray diffractograms (Figure 2) of C_{20}/C_{12} -PAM blend taken at 30°C are characteristic of a quite large number of additional sharp reflections arising from the crystalline structure of C_{20} . In a separate study it was confirmed that this diffractogram is nothing else than just a superposition of the two diffractograms of C_{12} -PAM and C_{20} , meaning that at 30°C C_{12} -PAM is not miscible with C_{20} at all. This complete immiscibility is natural, because at 30°C both the side chain and the C_{20} are crystalline.

At 110°C C_{20} (m.p. = 36–38°C) is molten, increasing the intensity of amorphous halo in the diffractogram of the C_{20}/C_{12} -PAM blend. Except for this change there is little difference between the diffractograms of pure C_{12} -PAM and C_{20}/C_{12} -PAM blend. As mentioned in our previous paper¹⁴, at 110°C the side chain crystals are, in spite of their high *gauche* content¹⁵, not molten yet. Therefore, C_{12} -PAM cannot be miscible with C_{20} even at 110°C.

At 140°C there occur drastic changes in X-ray diffractograms of both pure C_{12} -PAM and C_{20}/C_{12} -PAM blend. Since at this temperature the side chain crystals of C_{12} -PAM are completely molten, the peaks arising from these crystals are not observed any more and the intensity of the amorphous halo is increased in the wide-angle region of the diffractogram of C_{12} -PAM. But at 140°C its layered structure is not disrupted yet, and the reflection B attributed to the lateral backbone spacing is still observed in the diffractogram of C_{12} -PAM. In the wide-angle region of the diffractogram of C_{20}/C_{12} -PAM blend the same phenomenon is revealed as in pure C_{12} -PAM, but in its small-angle region it is seen that the reflection A of the blend is shifted to a smaller angle than that of pure C_{12} -PAM. This indicates that the layer spacing of the blend is larger than that of C_{12} -PAM. This increase in layer spacing must result from the penetration of C_{20} into the molten side chain domain of C_{12} -PAM, indicating clearly that there is a miscibility between molten side chains and C_{20} at 140°C.

In Figure 3 are reproduced temperature dependences of layer spacing of pure C_{12} -PAM and C_{20}/C_{12} -PAM blend (1/1 w/w). The upper curve denotes variation of the layer spacing of C_{20}/C_{12} -PAM blend and the lower one denotes that of pure C_{12} -PAM. From the lower curve it is seen that the layer spacing jumps suddenly at about 120°C. This jump temperature exactly coincides

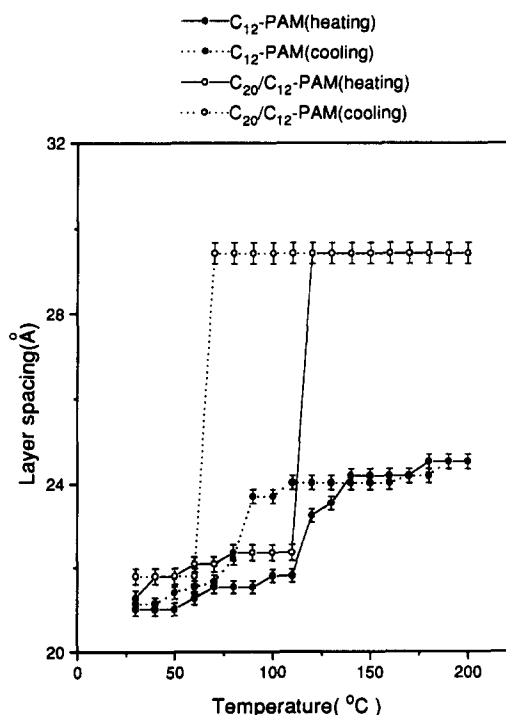


Figure 3 Temperature dependence of the layer spacing of C_{12} -PAM, C_{20}/C_{12} -PAM blend. The layer spacings are measured by WAXS

with the crystal–mesophase transition temperature measured by d.s.c., indicating that at this point the side chain crystal begins to melt and the C₁₂-PAM transforms into mesophase from crystalline phase. The lower curve of Figure 3 also shows that once mesophase is formed, neglecting the small increase resulting from the thermal expansion, layer spacing does not change with temperature. This behaviour indicates that there is no miscibility between the molten side chains and the rigid backbones in this temperature range, because the rigid backbones aligned regularly are not disrupted yet but still remaining.

The presence of the sudden jump in layer spacing for C₂₀/C₁₂-PAM blend can be observed also in the upper curve of Figure 3. But the jump for the blend is far higher than that for pure C₁₂-PAM. This jump occurs from miscibility between C₂₀ and C₁₂-PAM, both of which have nearly the same chemical structure. This phenomenon indicates that at the jump temperature C₂₀ begins to penetrate into the side chain region of C₁₂-PAM. The penetration should increase layer spacing and accordingly increase the volume of the side chain domain. To investigate how much C₂₀ can penetrate, the increments in layer spacing were measured for the other blends with 1/2 and 2/1 (w/w) C₂₀/C₁₂-PAM ratios. Contrary to our expectation, these blends exhibited the same increment as the 1/1 blend, even though the blend ratios had been remarkably changed. This constant increment indicates that an excess of C₂₀ was added to all three blends prepared and a solubility limit exists in the blend systems. Here the solubility limit is defined by saturated volume fraction of C_k penetrated into the side chain domain against the total volume of the miscible phase of the blend. As confirmed from Figure 3, this limit is independent of temperature in the measured 120–200°C range and of C_k composition in the measured 1/2–2/1 range. In fact, this limit could also be observed in all the other C_k/C_m-PAM blends, and in Figures 4 and 5 the layer spacing values obtained are plotted against the chain length of C_k and side chain length of C_m-PAM, respectively. As Figure 4 shows, the equilibrium values of layer spacing decrease with increasing C_k chain length, while, as Figure 5 shows, those sharply increase with increasing side chain length of C_m-PAM. Such a solubility limit was also observed in many binary blends of A homopolymer/AB block copolymer having lamellar morphology^{16,17}.

To determine the solubility limit values out of the layer spacing values measured experimentally, a simple geometrical calculation¹⁸ is taken into account. First let the solubility limit Φ_k be defined as

$$\Phi_k = V_k/V_T \quad (1)$$

where V_k is saturated volume of C_k dissolved in the side chain domain and V_T is total volume of the miscible phase of C_k/C_m-PAM blends. Since *n*-alkanes added to C_m-PAM dissolve only in the side chain region of C_m-PAM, the layer spacing d measurable for miscible phase of C_k/C_m-PAM blends can be given by the following equation from a simple geometrical consideration¹⁸.

$$d = \frac{d_m}{(1 - \Phi_k)(1 - f_s)} \quad (2)$$

where d_m is width of main chain of C_m-PAM, Φ_k is

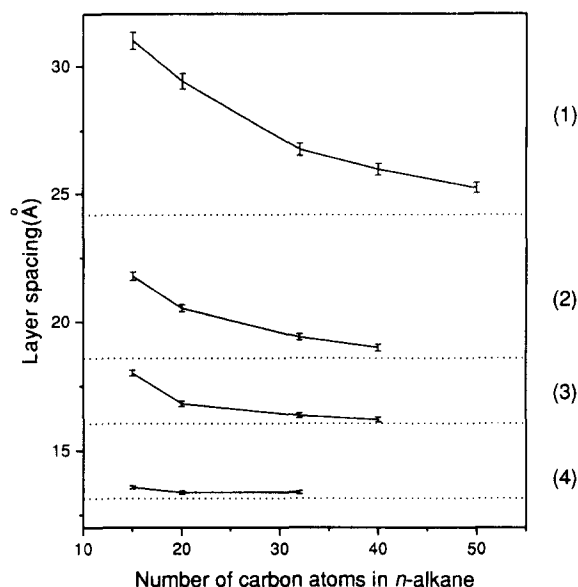


Figure 4 Layer spacing of C_k/C_m-PAM blends as a function of number of carbon atoms in *n*-alkane. (—): (1) C_k/C₁₂-PAM at 150°C; (2) C_k/C₈-PAM at 180°C; (3) C_k/C₆-PAM at 200°C; (4) C_k/C₄-PAM at 260°C. (·····): C_m-PAM; C₁₂-PAM (top) at 150°C, C₈-PAM at 180°C, C₆-PAM at 200°C and C₄-PAM (bottom) at 260°C

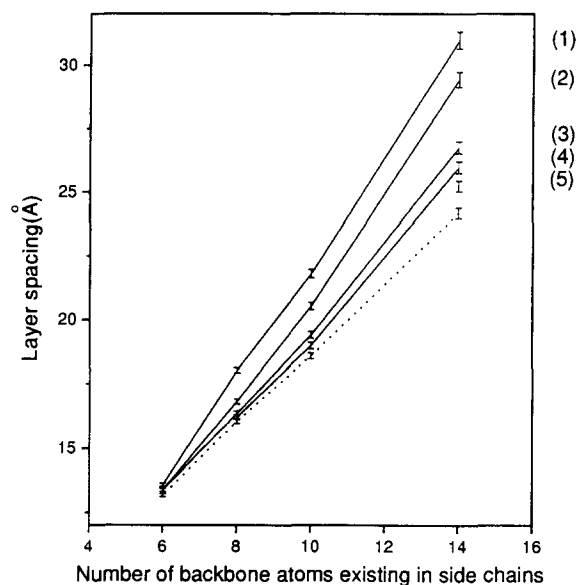


Figure 5 Layer spacing of C_k/C_m-PAM blends as a function of number of backbone atoms existing in side chains. (—): (1) C₁₅/C_m-PAM; (2) C₂₀/C_m-PAM; (3) C₃₂/C_m-PAM; (4) C₄₀/C_m-PAM; (5) C₅₀/C_m-PAM. (·····): C_m-PAM. The measured temperatures are the same as those in Figure 4

solubility limit of *n*-alkanes defined as above, f_s is volume fraction of side chain domain of C_m-PAM. We can solve equation (2) for Φ_k and get

$$\Phi_k = \frac{d(1 - f_s) - d_m}{d(1 - f_s)} \quad (3)$$

According to the crystallographic data of benzylidene-aniline¹⁹ having very similar chemical structure to the unsubstituted monomer of C_m-PAM, d_m is about 4.8 Å. This calculated value coincides approximately with the intercept value 4.7 Å in the plot¹⁴ of layer

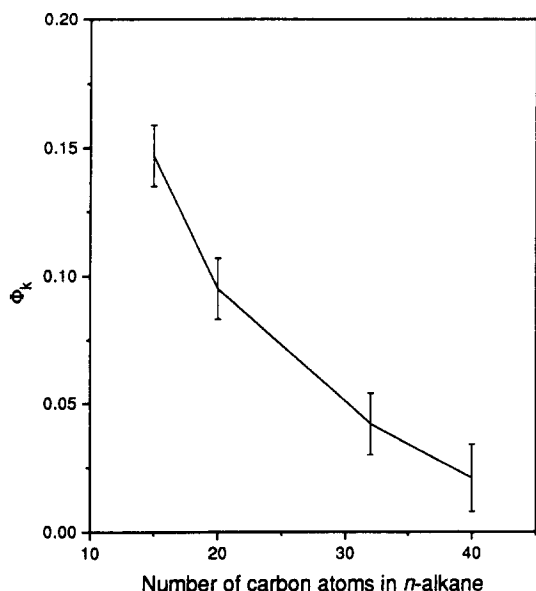


Figure 6 Solubility limit of *n*-alkane in C_k/C_8 -PAM blends as a function of number of carbon atoms in *n*-alkane

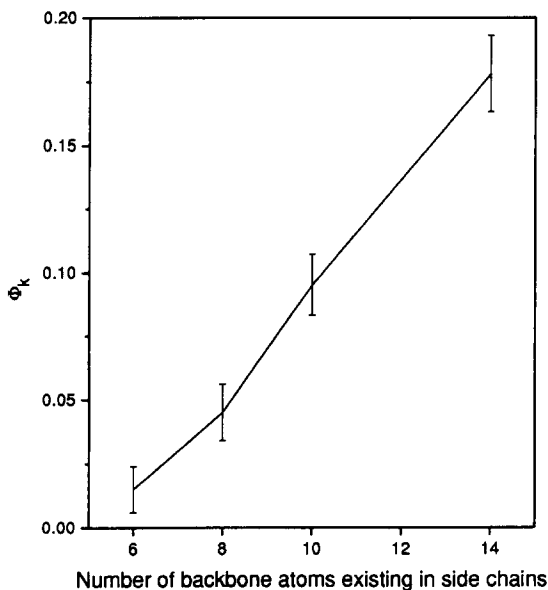


Figure 7 Solubility limit of *n*-alkane in C_{20}/C_m -PAM blends as a function of number of backbone atoms existing in side chains

spacings as a function of the length of side chain, as measured in mesophase. This value may be assumed not to change with side chain length of C_m -PAM or on blending C_k .

In Figures 6 and 7 the solubility limit values of C_k (Φ_k) thus obtained for C_k/C_8 -PAM and C_{20}/C_m -PAM blends are plotted against chain length of C_k and side chain length of C_m -PAM, respectively. Since other C_k/C_m -PAM blends showed similar features to the blends, only the solubility limit values of the blends are reproduced as representative examples. As Figure 6 shows, Φ_k decreases with increasing chain length of C_k . This is natural to understand, because the entropy of mixing decreases

with increasing chain length of *n*-alkanes and between the two components there is no specific chemical interaction leading to an increase in enthalpy of mixing. Figure 7 shows that Φ_k increases sharply with increasing side chain length of C_m -PAM. This results from the fact that the increase in side chain length naturally accompanies an increase in side chain content, and the more side chains there are, the more *n*-alkane is dissolved.

CONCLUSION

In C_k/C_m -PAM blend, liquid *n*-alkanes were miscible with the side chains of C_m -PAM and penetrated into their domain only when the side chains were molten to form mesophase. In mesophase the layered structure was not disrupted by adding C_k and on adding excess *n*-alkanes the presence of solubility limits was confirmed. With increasing side chain length of C_m -PAM and chain length of C_k the solubility limit of *n*-alkane increased and decreased, respectively. This behaviour is analogous to that of binary blends of A homopolymer/AB block copolymer having lamellar morphology.

ACKNOWLEDGEMENT

This work was supported by the Korea Science and Engineering Foundation (92-48-00-01).

REFERENCES

- 1 Ballauff, M. *Makromol. Chem. Rapid Commun.* 1986, **7**, 407
- 2 Ballauff, M. *Macromolecules* 1986, **19**, 1366
- 3 Ballauff, M. and Schmidt, G. F. *Mol. Cryst. Liq. Cryst.* 1987, **147**, 163
- 4 Berger, K. and Ballauff, M. *Mol. Cryst. Liq. Cryst.* 1988, **157**, 109
- 5 Ballauff, M., Rosenau-Eichin, R. and Fischer, E. W. *Mol. Cryst. Liq. Cryst.* 1988, **155**, 211
- 6 Rodriguez-Parada, J. M., Duran, R. and Wegner, G. *Macromolecules* 1989, **22**, 2507
- 7 Harkness, B. R. and Watanabe, J. *Macromolecules* 1991, **24**, 6759
- 8 Stern, R., Ballauff, M., Lieser, G. and Wegner, G. *Polymer* 1991, **32**, 11
- 9 Galda, P., Kistner, D., Martin, A. and Ballauff, M. *Macromolecules* 1993, **26**, 1595
- 10 Steuer, M., Horth, M. and Ballauff, M. *J. Polym. Sci. Part A: Polym. Chem.* 1993, **31**, 1609
- 11 Watanabe, J., Harkness, B. R., Sone, M. and Ichimura, H. *Macromolecules* 1994, **27**, 507
- 12 Kriecheldorf, H. R. and Domschke, A. *Macromolecules* 1994, **27**, 1509
- 13 Park, S.-B., Kim, H., Zin, W.-C. and Jung, J. C. *Macromolecules* 1993, **26**, 1627
- 14 Kim, H., Park, S.-B., Jung, J. C. and Zin, W.-C. *Polymer* in press
- 15 Whittaker, A. K., Falk, U. and Spiess, H. W. *Makromol. Chem.* 1989, **190**, 1603
- 16 Inoue, T., Soen, T., Hashimoto, T. and Kawai, H. *Macromolecules* 1970, **3**, 87
- 17 Ptaszynski, B., Terrisse, J. and Skoulios, A. *Makromol. Chem.* 1975, **176**, 3483
- 18 Skoulios, A. E. 'Developments in Block Copolymers', (Ed. I. Goodman), Ch. 3, Applied Science Publishers, London, 1982
- 19 Burgi, H. B. and Dunitz, J. D. *Helv. Chem. Acta* 1970, **53**, Fasc. 7, 206